Emission Modeling of an Interturbine Burner Based on Flameless Combustion

Perpignan, André A.V.; Talboom, M.G.; Levy, Yeshayahou; Rao, Arvind Gangoli

DOI
10.1021/acs.energyfuels.7b02473

Publication date
2018

Document Version
Final published version

Published in
Energy & Fuels

energy&fuels

Article

Cite This: Energy Fuels 2018, 32, 822−838

pubs.acs.org/EF

Emission Modeling of an Interturbine Burner Based on Flameless Combustion

André A. V. Perpignan,[†] Mathijs G. Talboom,[†] Yeshayahou Levy,[‡] and Arvind Gangoli Rao*[,†]

[†]Faculty of Aerospace Engineering, Delft University of Technology, Kluyverweg 1, 2629 Delft, The Netherlands

[‡]Turbo and Jet Engine Laboratory, Faculty of Aerospace Engineering, Technion, Haifa 32000, Israel

ABSTRACT: Since its discovery, the flameless combustion (FC) regime has been a promising alternative to reduce pollutant emissions of gas turbine engines. This combustion mode is characterized by well-distributed reaction zones, which potentially decreases temperature gradients, acoustic oscillations, and NO_x emissions. Its attainment within gas turbine engines has proved to be challenging because previous design attempts faced limitations related to operational range and combustion efficiency. Along with an aircraft conceptual design, the AHEAD project proposed a novel hybrid engine. One of the key features of the proposed hybrid engine is the use of two combustion chambers, with the second combustor operating in the FC mode. This novel configuration would allow the facilitation of the attainment of the FC regime. The conceptual design was adapted to a laboratory scale combustor that was tested at elevated temperature and atmospheric pressure. In the current work, the emission behavior of this scaled combustor is analyzed using computational fluid dynamics (CFD) and chemical reactor network (CRN). The CFD was able to provide information with the flow field in the combustor, while the CRN was used to model and predict emissions. The CRN approach allowed the analysis of the NO_x formation pathways, indicating that the prompt NO_x was the dominant pathway in the combustor. The combustor design can be improved by modifying the mixing between fuel and oxidizer as well as the split between combustion and dilution air.

1. INTRODUCTION

Aviation is a major player in the world economy, and it is growing steadily. It is expected to grow at a rate of 4.7% annually for the next couple of decades.[1] Add to this the rising fuel costs and the growing global pressure on the aviation industry to reduce its environmental impact, and it becomes obvious that the aviation community should design better and efficient aircraft for the future.

The anticipated reduction at various fronts (noise, air pollution, and fuel consumption) required to meet the future challenges, as envisioned by the Advisory Committee for Research in Aeronautics (ACARE) is shown in Figure 1. It can be seen that from an emission reduction point of view, reduction in CO_2, noise, and NO_x emissions are the most prominent. The aim is to reduce the CO_2 and NO_x emissions are reduced by 75% and 90%, respectively, by the year 2050 when compared to a typical aircraft in the year 2000.

Alternatives to gas turbines in aviation are still underdeveloped and will not become feasible in commercial aircraft for next several decades.[3] Consequently, a few approaches have been investigated to reduce the emissions from aero engines, which include cycle innovations, alternative fuels, novel combustion techniques, or a combination of these.

Some of the promising combustion techniques that are being investigated for gas turbines include lean direct injection (LDI), trapped vortex combustor (TVC), and flameless combustion (FC). Among these alternatives, FC regime is attractive due to its well-distributed reaction zone, which yields low-temperature gradients, low NO_x emissions, higher combustion stability, and low acoustic oscillations.[4,5]

However, the conditions required to attain the FC regime are not trivial in a gas turbine engine. The required preheating of the reactants and lower O_2 concentration present a challenge to the designers. A number of concepts and designs to employ FC in gas turbines have been proposed, simulated, or tested.

Gas turbine combustor design attempts intended to operate in the FC regime often rely on the internal recirculation of combustion products within the combustion chamber. Unlike furnaces in an industrial environment, there is no straightforward solution for preheating and dilution of reactants in a gas turbine. Gas turbine combustors are significantly different from industrial furnaces, as they have to operate at low overall equivalence ratios, have much higher heat density with low residence times, exhibit a wide operational range, operate at high pressure and limited volume, and have strict pressure-drop limits. Thus, one of the main challenges is to design a combustor that is able to promote mixing at required rates without excessive pressure losses and within the limited volume available.

1.1. Background.

The adopted strategies to recirculate vitiated combustion gases internally within a combustor can be divided into two categories: (i) jet-induced and (ii) geometry-induced recirculation. Both strategies showed difficulties regarding operational range, narrow low emissions windows, combustion efficiency, or integration within the engine.

In the first category, the FLOX type combustors are the most-explored configuration. The concept of these burners relies on high-momentum partially premixed jets to promote the mixing of the incoming reactants and recirculated combustion products. The fuel is injected through radially

Received: August 23, 2017
Revised: October 24, 2017
Published: November 21, 2017

DOI: 10.1021/acs.energyfuels.7b02473
Energy Fuels 2018, 32, 822−838

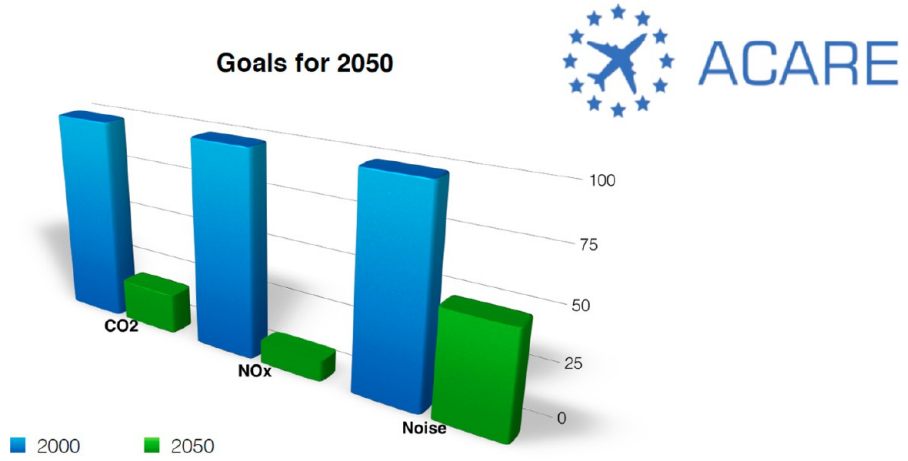

Figure 1. ACARE goals for emission reduction.[2]

distributed nozzles in a prechamber section, where it is partially premixed with the oxidizer. Both fuel and oxidizer promptly enter the combustion chamber through larger nozzles, positioned on the same axes as the fuel nozzles.

The first investigations under high-pressure conditions pointed to issues regarding pressure losses as the low emissions window could only be extended by increasing the jets momenta.[6] Furthermore, the energy density was lower than that of a conventional gas turbine combustor. Attempting to tackle the problems of low energy density and narrow operational range, the usual FLOX was redesigned using a nonpremixed configuration with the oxidizer being injected as coflow to each fuel jet,[7] allowing larger fuel mass flow rates. Another attempt involved having each of the premixing tubes fed by two fuel nozzles placed in the same plane and radial coordinate.[8] The concept aimed at extending the power modulation by regulating the fuel distribution between the nozzles.

Although these attempts were reported to have better results compared to the baseline design, further investigations were not performed (or published). Instead, an approach having a swirler-stabilized flame in the center of the FLOX combustor was presented and tested.[9,10] The architecture would operate similarly to a conventional combustor in its center, providing more freedom by splitting the air between the FLOX and the swirler burner. The investigations were promising, in spite of the relatively high CO emission. As the combustor was tested at atmospheric pressure, more-detailed investigations would be required to prove the design, especially in terms of pressure losses.

The FLOX concept was created for gaseous fuels. However, because liquid fuels are important to gas turbine applications, the use of liquid fuels has been recently investigated. Zizin et al.[11] tested possible configurations and designs that would allow the use of liquid fuels. Different atomizers and nozzles were tested for both single-nozzle and 12-nozzle configuration. The authors reported no clear advantage of one type of atomizer or nozzle over the others. The study was extended to an 8-nozzle configuration intended to operate in micro gas turbines,[12] and the conclusion was that the atomizers could easily be incorporated in the FLOX concept because of the large ratio between the air nozzle and atomizer diameter. However, the typical problems encountered using gaseous fuels were present: a too-limited operational range and a narrow low-emissions window.

In the studies mentioned above, the integration of the combustor within the gas turbine has not been discussed in details, and the principle of mixing is more suited for can-type combustors, which is not used in modern aero engines. Therefore, the future and applicability of FLOX-based gas turbine combustor is still uncertain. Furthermore, a range of other variations relying on jet-mixing is present in the literature and has been summarized by Arghode and Gupta.[13] The difficulties faced by such configurations are similar to those faced by the FLOX configuration.

The other approach investigated for FC in gas turbine is based on the creation of large recirculation zones by using the combustor geometry.[14−20] This strategy was adopted by the FLOXCOM[14−16] project, which was conceptually designed with aid of Chemical Reactor Networks (CRNs). The FLOXCOM had an annular shape, as most of the modern gas turbine combustors, representing an advantage over the FLOX concept.

An adapted prototype having a 60° sector of the full annular combustor was tested.[17] Diverse configurations of air inlets were tested, as the position and direction of the injection showed to have great influence on the performance. Recirculation ratio and pollutant emissions are sensitive to the air inlet design. Although the experiments did not assess the pressure losses, they are probably also dependent on such design choices.

In another work, the velocity and turbulent kinetic energy fields within the FLOXCOM were investigated.[18] Additionally, point measurements of temperature and main species were performed. Relatively uniform temperature profiles were identified, pointing to a successful attainment of the FC regime. The experiments showed low NOx emissions, while CO emissions and combustion efficiencies were not at satisfactory levels. The authors suspected that the residence times within the combustion zone were too low and that this could be overcome by changing dimensions or fuel injection location. However, gas turbine engines have severe constraints regarding the combustor volume, which could make it difficult to attain sufficiently high residence times.

1.2. Motivation. In view of the difficulties faced by both strategies, an alternative was proposed in the Advanced Hybrid Engines for Aircraft Development (AHEAD) project.[19,20]

DOI: 10.1021/acs.energyfuels.7b02473
Energy Fuels 2018, 32, 822−838

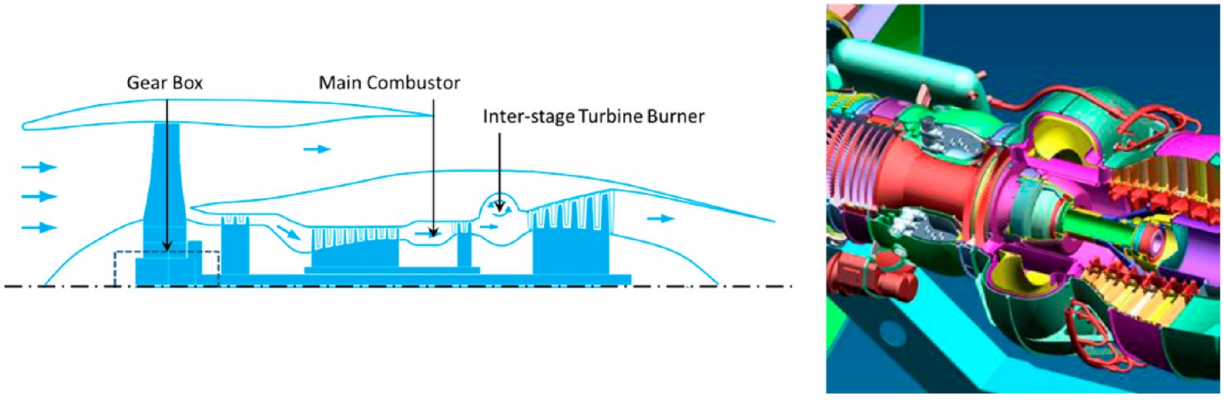

Figure 2. Dual-combustor engine concept presented along with the AHEAD project (left).[19] Cut-view of the ITB on the full engine structure. Right panel: Copyright 2014 Pratt and Whitney Rzeszów S.A.

Among other features, the project explored the advantages and challenges involved in having two sequential combustion chambers. The first and main combustion chamber would operate with fuels stored cryogenically, while the second would be an interturbine burner (ITB) intended to operate under the FC regime.

The benefit from the combustion point of view is that the gases entering the ITB would have high temperature and reduced O_2 concentration. Such conditions would ease the attainment of the FC regime, with possibly lower recirculation required and, therefore, lower pressure losses and required volume. Additionally, it has been shown that a dual-combustor gas turbine engine can be more efficient due to its off-design characteristics.[21]

The preliminary design of the FC combustor for a dual fuelled engine was presented by Levy et al.[22] and was based on chemical kinetics and computational fluid dynamics (CFD) analyses. The authors were able to dimension the combustor and estimate promisingly low emission values. An experimental model was developed based on their design and is discussed in the next section of the present work.

1.3. Modeling of Pollutant Emissions. The assessment and improvement of designs intended to operate under the FC regime is highly dependent on the model's ability to predict pollutant emissions because lower emissions are the main reason to pursue the FC regime. However, accurate modeling using CFD tools within reasonable computational costs for the design process is still challenging. The present analysis of the ITB is composed of two approaches that simplify the problem to reduce computational costs: CFD, along with simplified chemistry, and CRN, which neglects flow structures and turbulence−chemistry interaction. Evidently, both approaches have limitations and the study presented herein aims to evaluate the performance of the computational tools by comparing their predictions to experimental results and to provide insights into the design of the ITB by combining the results of both tools.

The use of CFD for assessing pollutant emissions is still challenging because many works point to inconsistencies in the comparison between simulations and experimental data. The lack of correct representation of the detailed chemistry has been pointed as the main source of inconsistency.[23] Due to this fact, approaches using CRNs have gained relevance, as chemistry can be modeled in detail while keeping the computational costs relatively low.

Fairly good results have been achieved by designing CRNs manually, determined based on experimental flow visualization or CFD simulations. The work of Park et al.[24] utilized a similar strategy as compared the one adopted in the present work. The resulting temperature, velocity and concentration fields from CFD calculations were used to determine the domain subdivisions within a lean-premixed gas turbine combustor. Similarly, Lebedev et al.[25] built a 6-reactor CRN based on the CFD predicted mixture fraction field. Again, their focus was on modeling pollutant emissions of a gas turbine combustor.

Other papers focused on postprocessing CFD solutions to define CRNs based on criteria to group computational cells into ideal reactors. Monaghan et al.[26] employed the solution of temperature and mixture fraction as well as the axial coordinate and tested their approach with the Sandia flame D. The authors were able to improve NO_x and OH predictions in relation to the initial CFD solution, while they performed a comprehensive analysis of the NO_x formation pathways in the D flame, another advantage enabled by the CRN approach.

Similar approaches were developed by Fichet et al.[27] and Cuoci et al.,[28] with algorithms dedicated to grouping cells based on the CFD solution to form CRN. Fichet et al.[27] simulated a conventional gas turbine combustor, while Cuoci et al.[28] compared the results to a test-case dedicated to investigating FC.[29] The reported results from the latter showed reasonable agreement for NO_x emissions, while CO was over-predicted.

The applicability of CRNs to assess emissions in the FC regime is better than in conventional combustion due to the inherent characteristics of the regime. Lower temperature and species gradients are closer approximations to the conditions of an ideal reactor. Therefore, the number of reactors required to simulate a given volume tend to be lower in FC.

2. COMBUSTOR CONCEPT AND EXPERIMENTS

Previous design attempts aimed at the application of FC to gas turbines faced several challenges, as discussed in section 1.1. To overcome such difficulties, the engine concept developed in the AHEAD project cosponsored by the European Commission, proposed a dual-combustor configuration (Figure 2), as presented by Rao et al.[19] The first combustor would operate on cryogenic fuels (LH_2 or LNG) The second combustor, located between the HPT and LPT, known as the ITB would operate with liquid hydrocarbon fuels (conventional or biofuels). This combustor can potentially achieve the FC regime as the incoming gases are already vitiated and are at high temperature.

DOI: 10.1021/acs.energyfuels.7b02473
Energy Fuels 2018, 32, 822−838

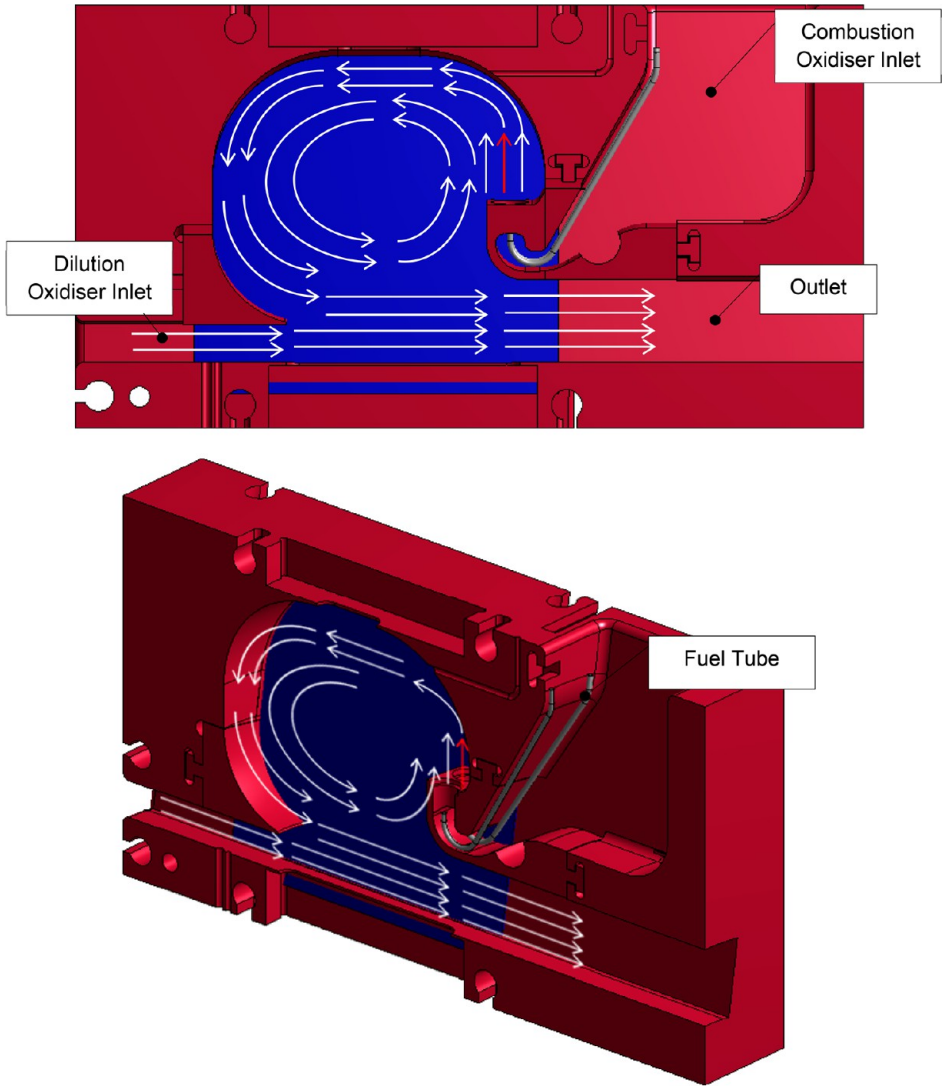

Figure 3. Geometry of the 18° combustor sector employed in the experiments. Geometry is cut in half along the longitudinal axis, with the quartz window depicted in blue.[30]

The conceptual design for the second combustor, described by Levy et al.,[22] relied on a large recirculation zone, similar to the FLOXCOM[14−16] configuration. Instead of the full annular combustor, the experimental campaign by the team in Technion employed an 18° rescaled section tested at atmospheric conditions. This experimental combustor sector contained three fuel ports (as the full annulus was designed to have 60 injectors). Part of the oxidizer entered the combustor along with the fuel (combustion oxidizer), in co-flows. The fuel injectors had 1 mm diameter, while the cylinders of oxidizer co-flows had 8.3 mm. The dilution oxidizer stream entered near the other end of the recirculation zone (see Figure 3).

Experiments were conducted at atmospheric pressure using CH_4 as fuel. The incoming air could be preheated, diluted with N_2, or diluted with H_2O (representing the product of combustion from the first combustion chamber using H_2). The laterals of the combustor had quartz windows, which were employed for visual inspection. The experiments aimed to understand the behavior of the combustor operating parameters on emissions, measured at the outlet of the combustor.

The combustor was tested for various equivalence ratio, N_2 and H_2O dilution levels. Conditions with oxidizer dilution were performed by maintaining air and fuel mass flows while adding different amounts of N_2 or H_2O to the oxidizer stream. The addition of H_2O was to emulate the vitiation of the gases as would happen in the dual combustion system. Equivalence ratio was altered by maintaining the fuel mass flow (5.91×10^{-5} kg/s) and changing the amount of air.

Photographs of the combustor with varying degree of N_2 dilution can be seen in Figure 4. It can be seen that apart from moving the reaction zone downstream due to the larger mass flow rates, N_2 addition increased the volume occupied by the reaction zone and increased the radiation from the combustor walls (relative to the flame region radiative emission), a common feature of FC regime as shown by Tu et al.[31] for example.

Emissions of CO and NOx for varying Φ, N_2, and H_2O addition are summarized in Figure 5. Interestingly, both CO and NO_x had nonmonotonic behavior with varying Φ, even though all conditions were in the lean region (Φ_{loc} ranged from 0.46 to 0.75). The local equivalence ratio (Φ_{loc}) is defined using the combustion oxidizer mass flow (excluding the dilution oxidizer). This behavior is further discussed and explained in section 4. The behavior with N_2 addition was in line with

DOI: 10.1021/acs.energyfuels.7b02473
Energy Fuels 2018, 32, 822−838

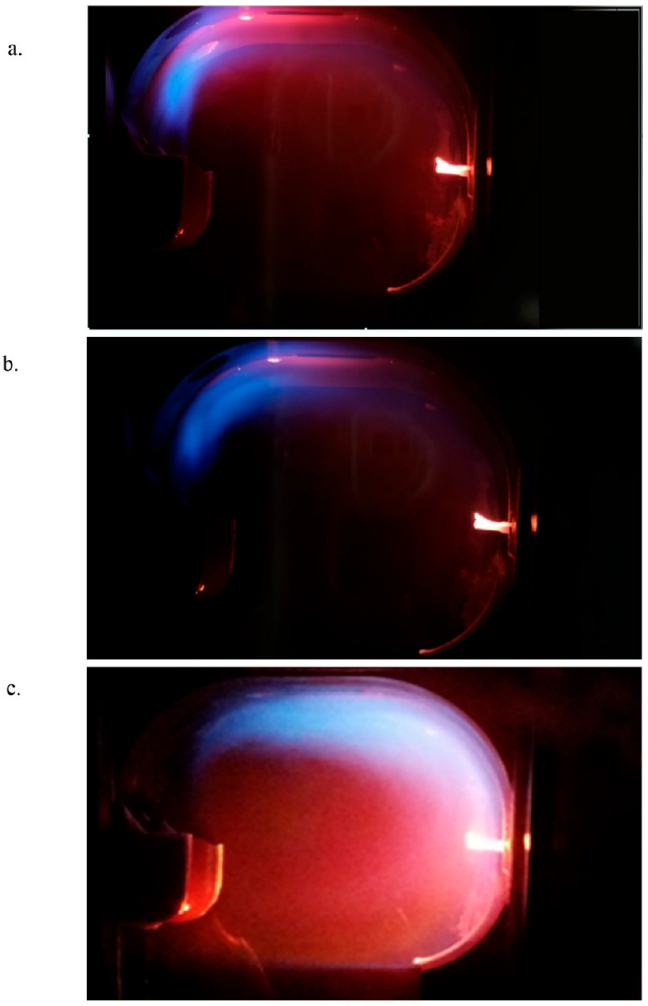

Figure 4. Photographs of the combustor for different amounts of N_2 addition.[30] For 0 l_n/min, 40 l_n/min and 100 l_n/min steps (from *a* to *c*). Fuel mass flow of 5.91×10^{-5} kg/s. The incandescent filament on the right side is a thermocouple. Please note that the photographs are meant for visual representation only.

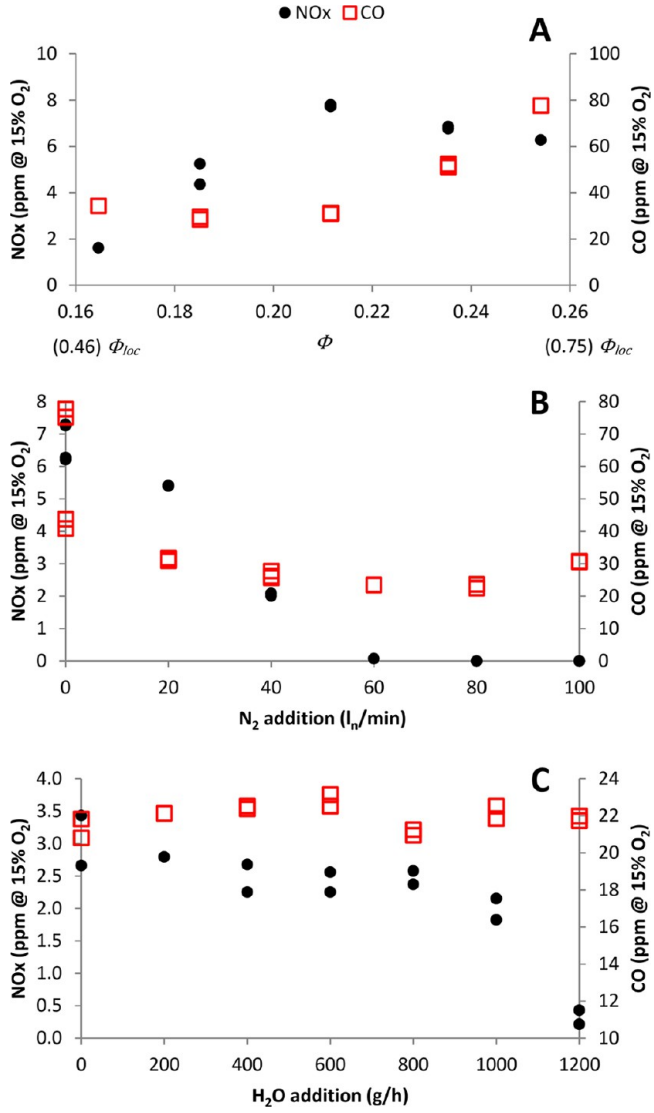

Figure 5. (A) Experimental results of NO_x and CO emissions with a variation of global equivalence ratio (values of local equivalence ratio also indicated), (B) N_2 addition to the oxidizer, and (C) H_2O addition to the oxidizer.[30]

previous studies[32] because NO_x decreased with increasing N_2, while CO increased after a certain level of dilution. The addition of N_2 can primarily have two effects; first is the reduction in the O_2 concentration (thereby reducing the peak temperatures), and the second effect is due to the reduction in the residence time. Water addition had little effect on the CO emissions, while it decreased NO_x emissions significantly. The modeling and analysis of the effect of H_2O addition will be treated in another publication. The details of the experimental campaign will be described in a separate publication by the team in Technion.

3. COMPUTATIONAL MODELING

The challenge of modeling reacting flows is often related to how simplifications and assumptions cause deviations in relation to the actual behavior and how these deviations vary for different conditions. Throughout the years, many studies have been dedicated to investigating the effect of possible simplifications on premixed and diffusion flames. Models able to yield good results across a broad range of operational conditions is still a major challenge in combustion research. Furthermore, combustion modeling is more often focused on predicting flame structures rather than pollutant emissions.

The modeling presented herein has several objectives:

1. understanding the effect of dilution and equivalence ratio on the flowfield and pollutant emission;
2. assess the performance of CFD regarding prediction of pollutant emissions using simplified chemistry;
3. assess the capabilities and limitations of CRNs in predicting emissions and in assisting the design; and
4. provide useful insights for improving the ITB concept by combing the information provided by the two modeling approaches.

The modeling setups are presented in the following subsections for CFD and CRN, respectively.

3.1. Computational Fluid Dynamics. The simulations are performed to assess the use of CFD to improve combustor design with respect to pollutant emissions. The Reynolds averaged Navier–Stokes (RANS) approach with flamelet generate manifolds (FGM)[33] is used. The FGM is used as its

DOI: 10.1021/acs.energyfuels.7b02473
Energy Fuels 2018, 32, 822–838

computational cost is considerably lower than other models (e.g., eddy dissipation concept and conditional source-term estimation). The approach allows the use of detailed chemistry in the flamelet calculations. The flamelets can be chosen to compose premixed or nonpremixed conditions. The mean turbulent flame structure is computed by means of the source terms of the laminar flames (or their state) and of ensemble averaging. The turbulence−chemistry interaction is taken into account with a presumed β shape probability density function (PDF), assumed to a mathematical function depending on the mean mixture fraction and its variance (eqs 1−3):

$$p(f) = \frac{f^{\alpha-1}(1-f)^{\beta-1}}{\int f^{\alpha-1}(1-f)^{\beta-1}\mathrm{d}f} \tag{1}$$

$$\alpha = \overline{f}\left[\frac{\overline{f}(1-\overline{f})}{\overline{f'^2}} - 1\right] \tag{2}$$

$$\beta = \left[\frac{\overline{f}(1-\overline{f})}{\overline{f'^2}} - 1\right] - \alpha \tag{3}$$

The employed FGM approach is based on the creation of a diffusion flamelets manifold that is accessed during the CFD calculations, based on the local values of the chosen control variables. Both adiabatic and nonadiabatic formulations were employed, having mixture fraction, a progress variable (c) and enthalpy (for the nonadiabatic case) as controlling variables. The heat balance performed taking the experimental data into account (temperatures at the inlet and at the outlet) suggested that the heat losses were not negligible, justifying the use of the nonadiabatic approach.

The diffusion flamelets are solved in the mixture fraction space for the species (eq 4) and for temperature (eq 5).

$$\rho\frac{\partial Y_i}{\partial t} = \frac{\rho\chi}{2}\frac{\partial^2 Y_i}{\partial f^2} + S_i \tag{4}$$

$$\rho\frac{\partial T}{\partial t} = \frac{\rho\chi}{2}\frac{\partial^2 T}{\partial f^2} - \frac{1}{c_p}\sum_i S_i H_i + \frac{\rho\chi}{2c_p}\left[\frac{\partial c_p}{\partial f} + \sum_i c_{p,i}\frac{\partial Y_i}{\partial f}\right]\frac{\partial T}{\partial f} \tag{5}$$

These equations are then transformed to the progress variable space. The effect of heat losses is only taken into account in burnt products, where the progress variable is equal to 1 and equilibrium is considered. Therefore, mass fractions for progress variable lower than 1 are not influenced by enthalpy variations, while temperatures are adjusted based on mean enthalpy values:

Most of the simulations employed a definition of progress variable dependent on CO_2 and CO mass fractions, as shown in eq 6. Attempts using the H_2O mass fraction to define the progress variable were investigated, but it did not improve the results. The diffusion flamelet manifolds were generated using GRI 3.0 chemical reaction mechanism.[34] Additionally, NO_x formation was modeled using transport equations for the mass fractions of NO, N_2O, NH_3, and HCN, with their source terms calculated via the thermal, prompt, and N_2O intermediate pathways, with presumed β-shape PDF to take temperature fluctuations into account:

$$c = \frac{(Y_{CO_2} - Y^{u}_{CO_2}) + (Y_{CO} - Y^{u}_{CO})}{(Y^{eq}_{CO_2} - Y^{u}_{CO_2}) + (Y^{eq}_{CO} - Y^{u}_{CO})} \tag{6}$$

All of the simulations were performed with the commercial code ANSYS Fluent. The standard k-ε turbulence model was employed as tests using the k-ω SST model and a Reynolds Stress turbulence model did not significantly change the results in terms of emissions. Along with the nonadiabatic approach, radiation was taken into account using the discrete ordinates model. The weighted sum of gray gases[35] was employed to calculate the radiative properties of the gases. Heat conduction through the walls was included by imposing an estimated outer wall temperature as well as their thicknesses and thermal properties. The properties of the quartz windows on the lateral domain was obtained from the work of Loenen and van der Tempel.[36]

The computational mesh was refined until no difference was spotted in the emissions and midplane fields (both temperature and velocity) for a chosen case. All meshes were hexahedral and the variation in the emissions as a function of mesh refinement can be seen in Figure 6. The employed computational mesh had approximately 5.6 million elements (Figure 7). The zone closest to the fuel injection port had finer refinement than other regions.

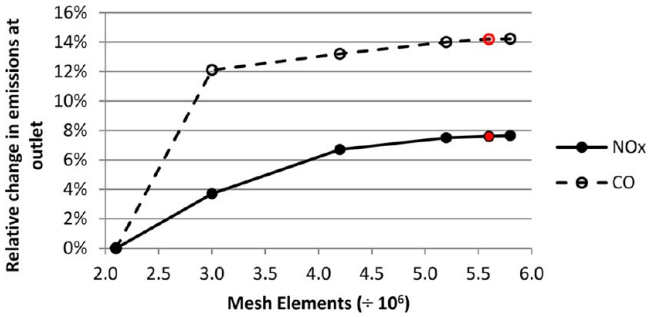

Figure 6. Variation in the emissions with mesh density (results for 2 100 000 elements as reference). Data points in red indicate the adopted mesh.

Mass flows and composition were imposed at the domain inflow boundaries with a turbulence intensity of 5%. The outlet boundary, where the resulting emission values were computed, was set to have zero mean relative pressure.

3.2. Flow-Field Analysis. The obvious advantage of CFD is the characterization of the flow field, which can provide useful information regarding the combustor design. The experimental campaign did not entail any flow field measurements and thereby did not provide experimental data for model validation.

The results suggest that the mixing between dilution air and the stream coming from fuel and combustion air is inadequate (Figures 8 and 9). The gradients persist until the domain outlet and show nearly no interaction between the two streams. This behavior was observed for all turbulence models. It is therefore clear that the interaction between the streams should be increased to improve mixing and to obtain the desired temperature pattern factor at the turbine inlet situated downstream of the combustor.

The plots also show an undesirable behavior: most of the reactions take place near the combustor walls and not in the recirculation zone, as was intended. This behavior would cause

DOI: 10.1021/acs.energyfuels.7b02473
Energy Fuels 2018, 32, 822−838

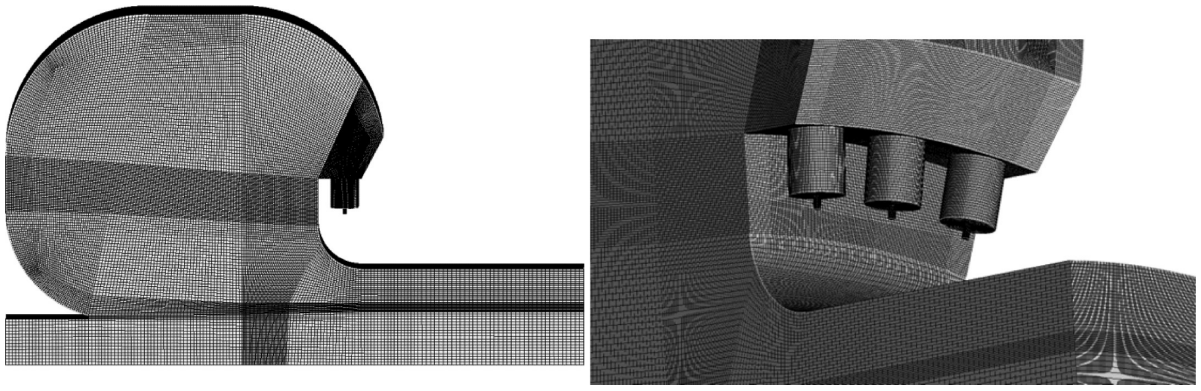

Figure 7. Computational mesh. Side view (left) and fuel injection region (right).

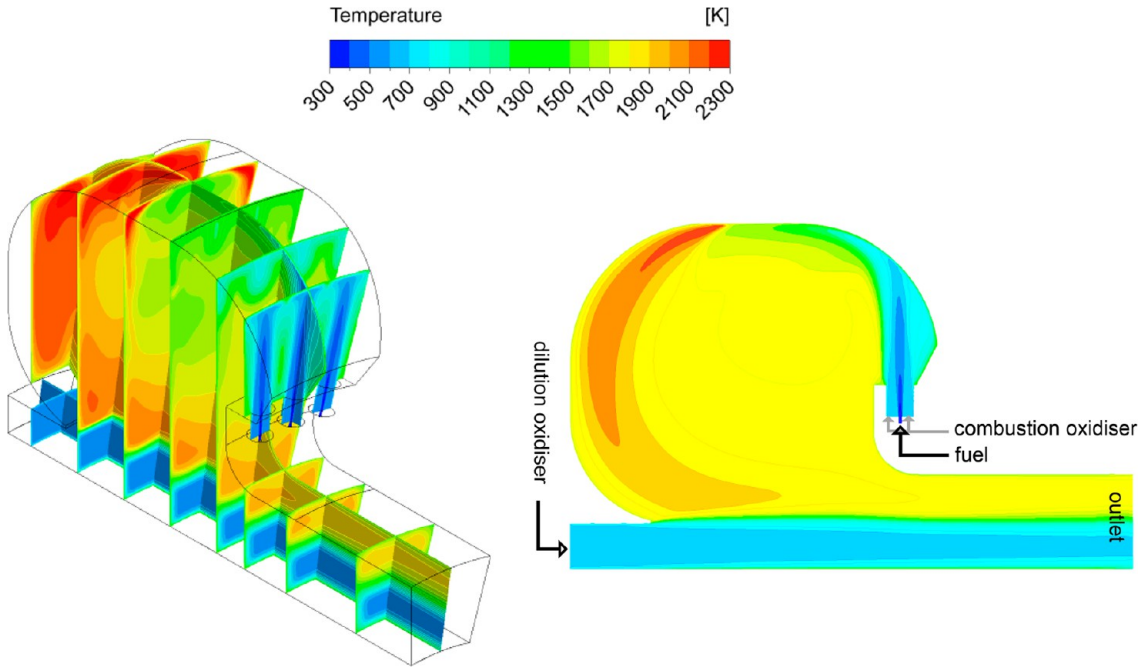

Figure 8. Temperature field with ϕ = 0.235. Nonadiabatic CFD simulations.

problems to the durability of the combustor walls (due to the complex flame-wall interaction) and would lead to increased CO emissions due to quenching.

To quantify the recirculation of combustion products, a recirculation ratio was calculated. Similar to the procedure adopted by Melo et al.,[17] the recirculation ratio R is defined by eq 7, in which A is the area of the surface shown in Figure 10. The surface was defined as follows: the center of the recirculation zone (where velocity is zero) in the central plane of the combustor was taken (shown by the dot in Figure 10). This point defined the upper limit of the vertical surface, while the horizontal surface was defined by the position where the flow split along the wall (highlighted in Figure 10):

$$R = \frac{\int_A \rho \mathbf{V}\cdot\mathbf{N}\mathrm{d}A}{\dot{m}_{\mathrm{oxid}} + \dot{m}_{\mathrm{fuel}}} \quad (7)$$

The defined R is therefore the ratio between the mass flow of recirculated products and the total mass flow rate. To neglect the effect of the dilution oxidizer stream, a local recirculation ratio (R_{loc}) is defined that takes into account the oxidizer mass flow rate injected along with the fuel.

The values of R and R_{loc} for different ϕ are shown in the plot of Figure 11. The overall values of R are low if compared to those of the FLOXCOM,[17] which were between 0.34 and 1.12. Although it makes more sense to compare these values to those of R_{loc}, as the FLOXCOM did not have any oxidizer split, the values on the range of 0.5 to 0.7 are also considered suboptimal to attain FC[5]. The most important conclusion that can be drawn from Figure 11 is that the dilution oxidizer stream has almost no influence on the recirculation: the trends of R and R_{loc} are similar, with the dilution stream slightly increasing R only for the highest values of ϕ. The recirculation is larger for lower ϕ due to the increase in the overall mass flow, which increases the jet momentum and, consequently, the induced recirculation.

By analyzing the resultant Da distribution from the CFD simulations (Figure 12), it can be seen that the Da decreases significantly (close to unity) with the addition of N_2. Thereby, supporting the fact that the combustor was operating in the FC regime during the experiments with high N_2 dilution, especially with 80 and 100 l_n/min N_2. The Da is pointed as an indicator of the FC regime.[37] Values of Da close to unity denote that neither chemistry nor mixing (or turbulence) is what limits and

DOI: 10.1021/acs.energyfuels.7b02473
Energy Fuels 2018, 32, 822−838

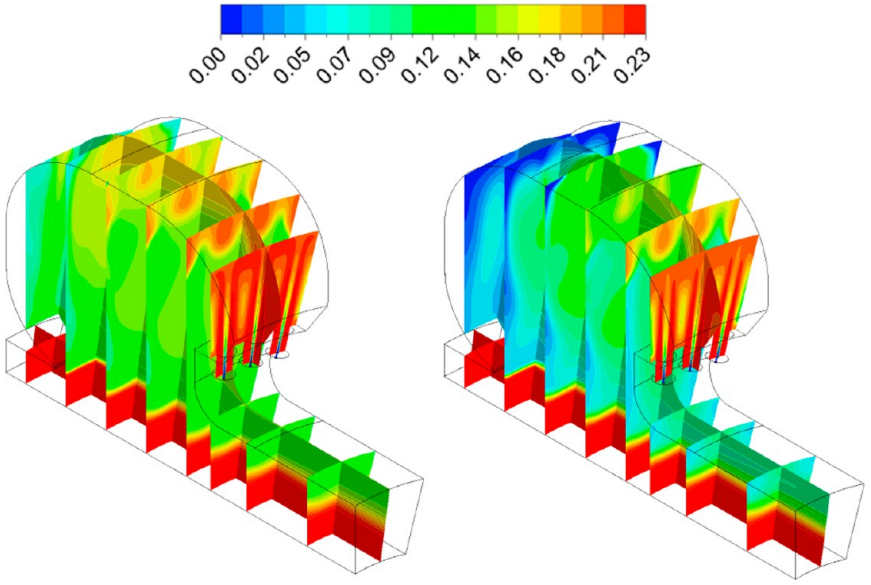

Figure 9. O_2 mass fraction for two different equivalence ratios with no air dilution. ϕ = 0.165 (left) and ϕ = 0.235 (right). Isometric view and nonadiabatic CFD simulations.

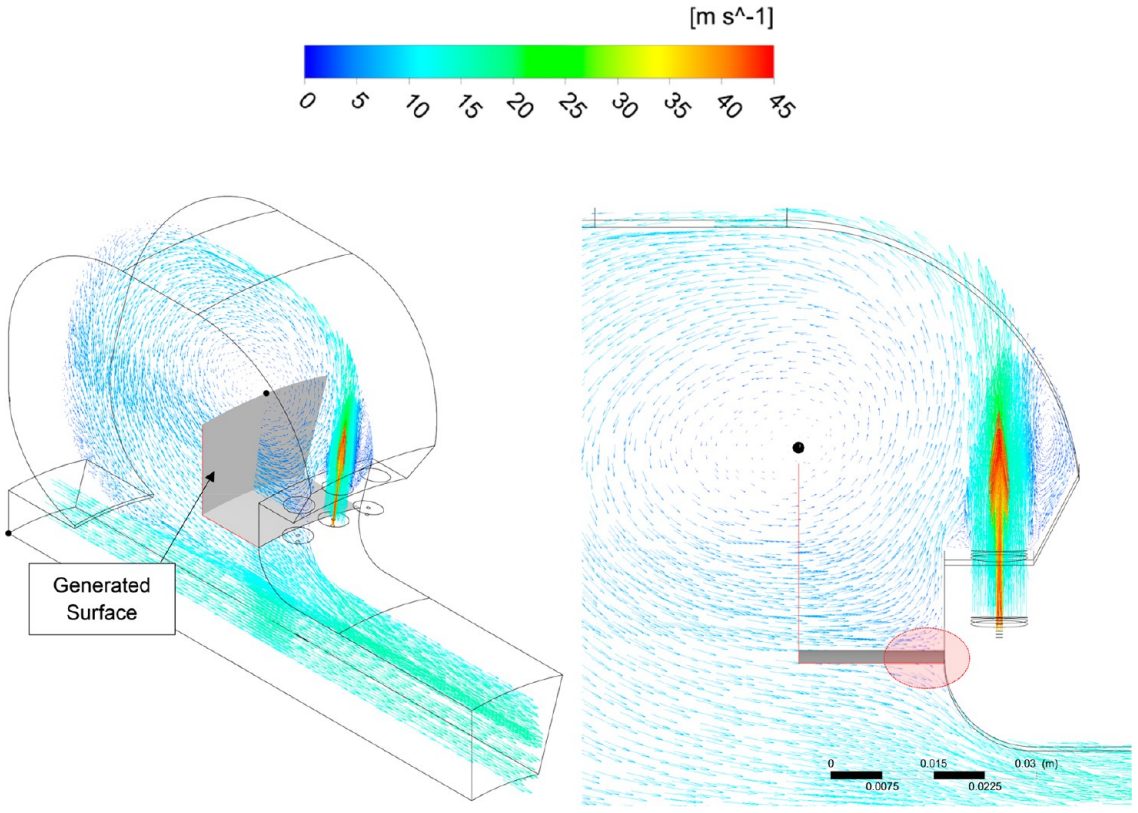

Figure 10. Example of a defined surface for the calculation of the recirculation ratio for the case with ϕ = 0.254. Velocity vectors on the central plane of the combustor. The dot depicts the center of the recirculation zone, where velocity is equal to zero. Isometric (left) and lateral view (right).

governs the reaction progress, as the two time-scales are comparable. The Da is calculated as shown in eq 10, where the formulation present in the Zimont model[38] is used to estimate the turbulence time-scale (eq 8):

$$\tau_t = \frac{l_t}{u'} = \frac{0.37(u'^3/\varepsilon)}{u'} = 0.37\left(\frac{2}{3}\right)\left(\frac{k}{\varepsilon}\right) \quad (8)$$

$$\tau_c = \frac{\alpha}{S_l^2} \quad (9)$$

$$\mathrm{Da} = \frac{\tau_t}{\tau_c} = \frac{0.37(2/3)(k/\varepsilon)}{\alpha/S_l^2} \quad (10)$$

The addition of N_2 lowers the values of Da, going from maximum values across the whole domain of above 20 (without N_2) to around 5 (with 80 l_n/min of N_2) and below 3 (with 100

DOI: 10.1021/acs.energyfuels.7b02473
Energy Fuels 2018, 32, 822−838

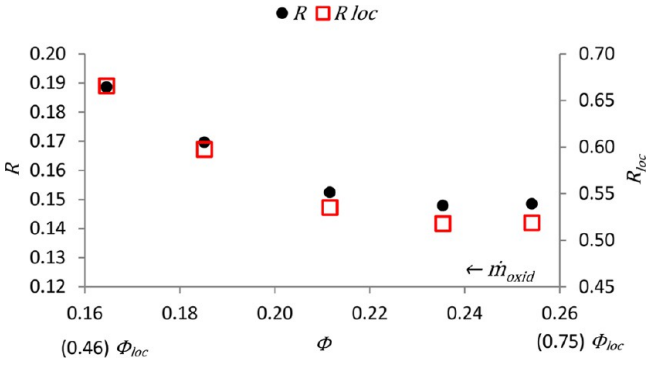

Figure 11. Recirculation ratio and local recirculation ratio as functions of the global equivalence ratio.

l_n/min of N_2). Mean Da values in the combustion zone (excluding the dilution air and exhaust regions) were close to unity in the case with 100 l_n/min of N_2. The simulations are supported by the photographs taken during the experiments (Figure 4). The blue regions in the photographs mark the reaction zones, which gradually move downstream with increasing N_2 addition. At the maximum level of N_2 addition (100 l_n/min − *c* on Figure 4), the photograph shows the most distributed reaction zone with increased red luminosity coming from the walls, a characteristic that is often observed when FC is attained. Moreover, the reaction zones are shown to be located along the combustor walls, as predicted by the simulations.

Given the results of both simulations and experiments, it is likely that the dilution of the oxidizer stream with N_2 shifts the combustor to the FC regime. It is worth considering that the attained level of dilution at the inlet during the experiments was lower than the predicted operational dilution of the dual-combustor system:[39] while the most diluted case shown in Figure 12 has 17.5% O_2 (mass), the ITB is predicted to operate between 10 to 15.5% O_2. Therefore, the attainment of the FC regime would be even more likely in the actual operation. In the actual application, H_2O is responsible for the dilution along with CO_2, in case CH_4 is employed in the main combustor. The different heat capacities between N_2, H_2O, and CO_2 may alter the behavior of the combustion zones for the same amount of dilution.

The comparison between different ϕ shows that the combustor performance may be greatly affected by the split between combustion and dilution air because the mixing between the two streams is not intense. While the lowest value of Φ in Figure 9 indicates an excess of O_2 throughout the whole combustor, the increase in Φ creates undesirable regions with no O_2. Although such prediction may be the reason for the overprediction of CO emissions discussed in section 3.4 (being therefore inaccurate), further studies should be performed to ensure that the designed air split is adequate for the whole operational range of the combustor.

3.3. Chemical Reactor Network. Because the main advantage of a successful gas turbine combustor designed to operate in the FC regime would be the lower pollutant emissions, it is important to have models able to predict them. However, CFD simulations are often not predictive enough. As discussed in the introduction, the use of CRNs has been pointed as one of the alternatives to predict emissions.

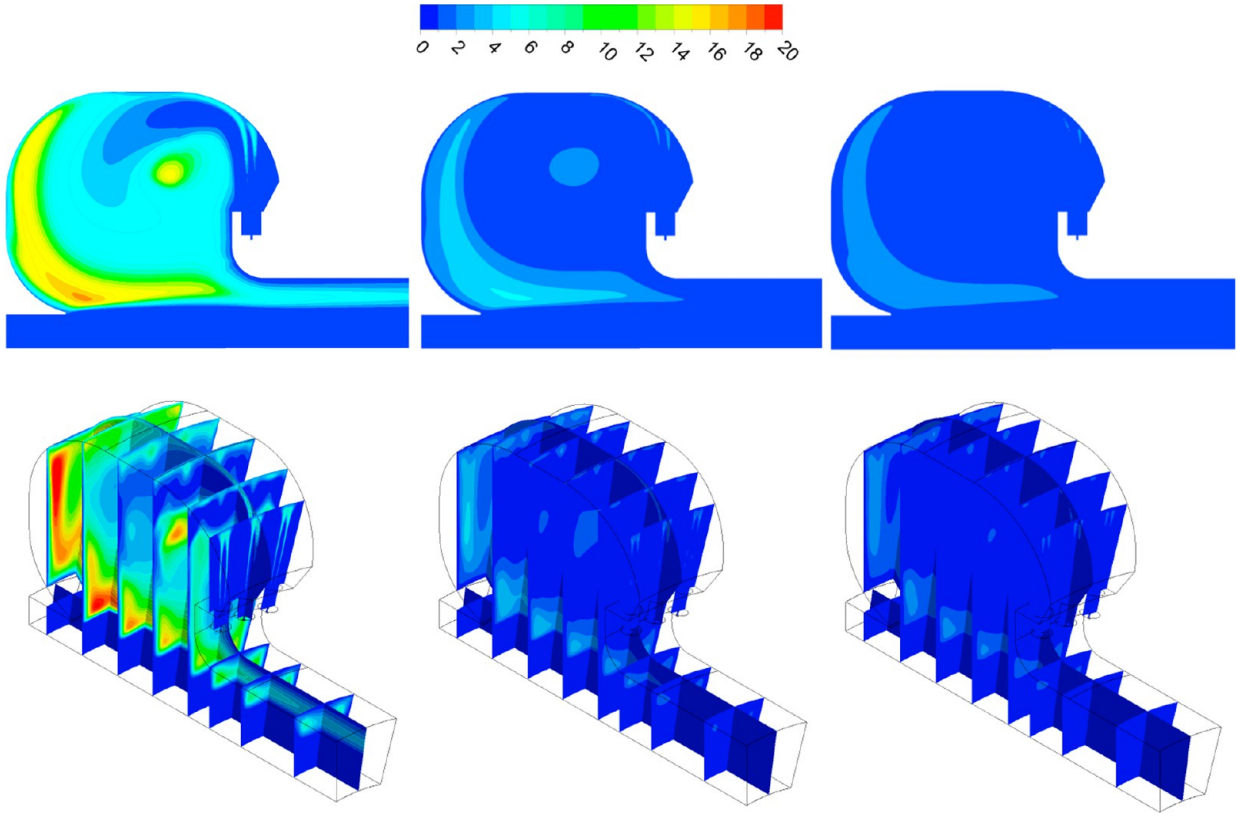

Figure 12. Calculated Da for the without nitrogen addition (left), with 80 l_n/min N_2 addition (middle) and 100 l_n/min (right). Lateral (up) and isometric (down) views. Nonadiabatic CFD simulations.

DOI: 10.1021/acs.energyfuels.7b02473
Energy Fuels 2018, 32, 822−838

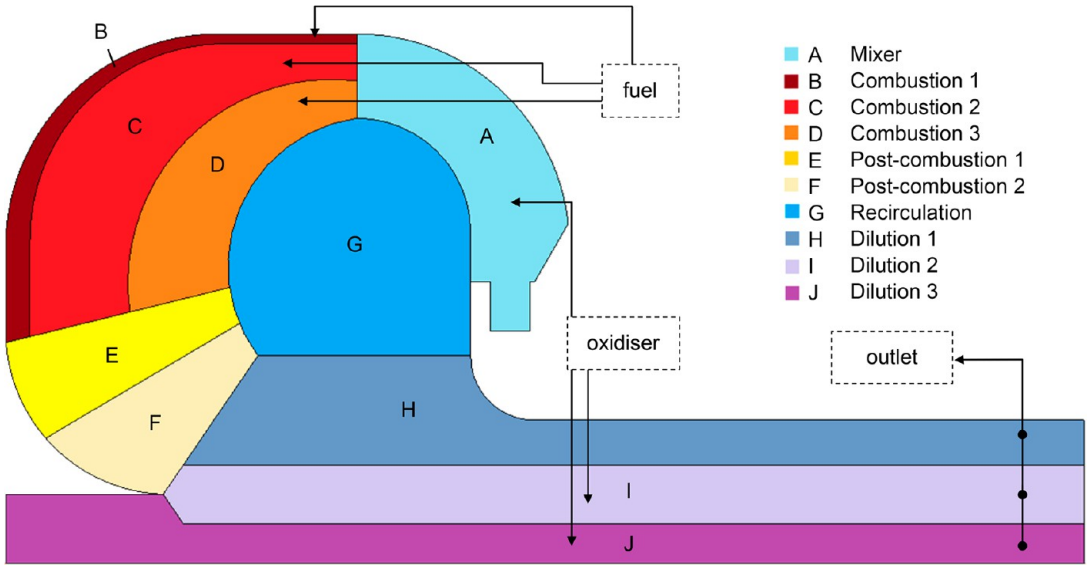

Figure 13. Regions of the interturbine combustor divided into idealized reactors in the designed CRN.

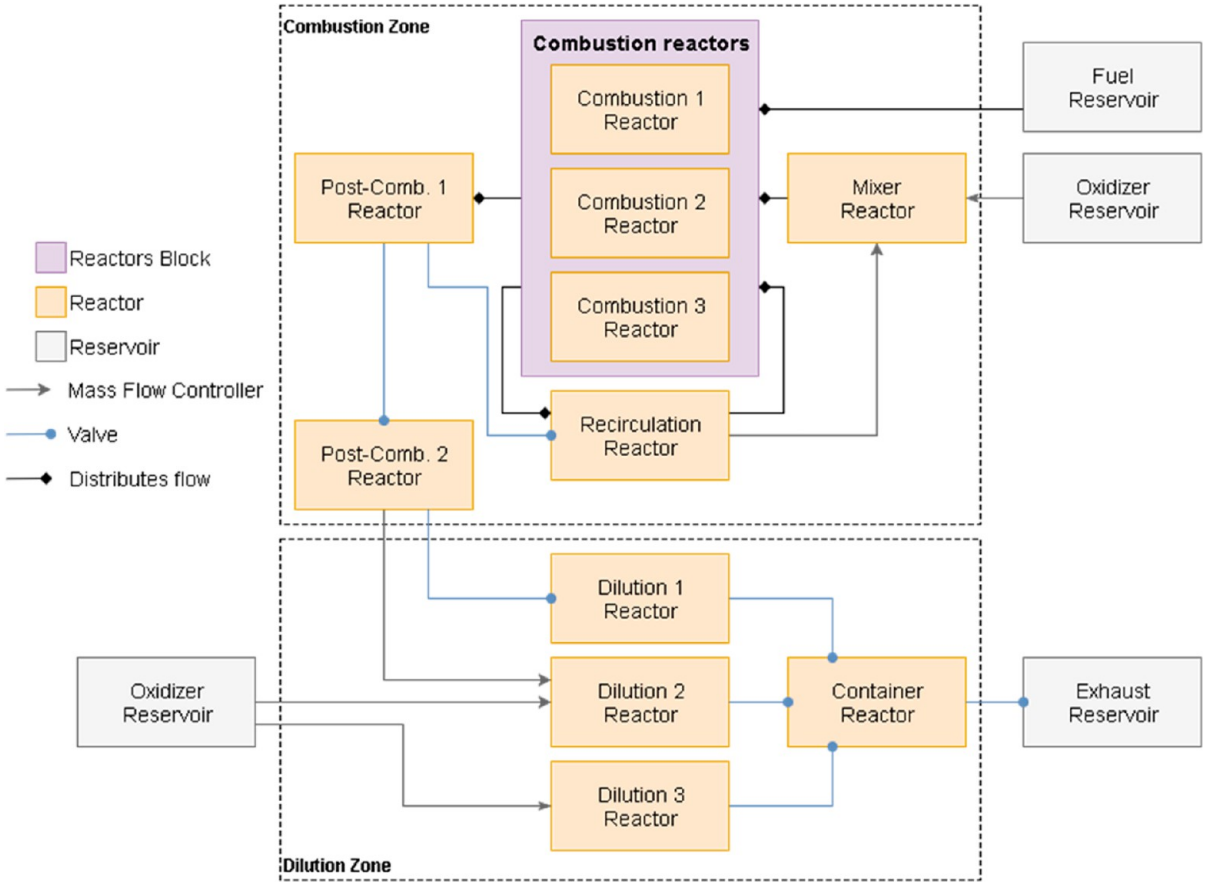

Figure 14. Structure of the designed CRN.

Having the flow field results from the CFD, a CRN was designed to represent the ITB. The combustor volume was subdivided into ideal reactors based on the temperature and composition gradients. The velocity field helped in determining the volume of the reactor representing the central recirculation zone. The amount of recirculation was also estimated by the composition and velocity fields.

After some iterations, the regions depicted in Figure 13 were established. Each region was represented by a perfectly stirred reactor (PSR). The CRN was modeled and solved using the open source code Cantera.[40] The connections between the reactors and the structure of the CRN can be seen in Figure 14. The given names to the reactors on Figures 13 and 14 represent the behavior observed in the CFD simulations in each region.

DOI: 10.1021/acs.energyfuels.7b02473
Energy Fuels 2018, 32, 822−838

Total heat losses were calculated based on the inlet and outlet temperatures measured during the experiments. Because the lateral windows were made of quartz and were much thinner than the other walls, it was assumed that conduction took place only across the lateral windows. Therefore, the allocation of heat loss was dependent on the temperature reached in each reactor and on their lateral areas.

The GRI 3.0 mechanism[34] was employed to determine reactions and their rates in the CRN. As previous works reported the tendency of this mechanism to overpredict NO_x emissions, the GRI 2.11[41] was also employed to draw a comparison, as literature indicates a better performance in terms of NO_x emission.[42−44] The difference between the two mechanisms is attributed to the different rates obtained for the prompt NO_x formation.

The CRN allows the analysis of each NO_x-formation pathway. The usual manner to account for the individual contributions relies on the deactivation of the reaction pathways. Essentially, three options have been discussed in the literature: (i) sequentially add the pathways and compare the output, (ii) sequentially remove the pathways,[45] and (iii) disable reactions of each pathway and compare to the output with all reactions enabled.[46] The latter was adopted in the present study because it requires disabling a lesser number of reactions and, therefore, potentially reduces error due to the interaction between the pathways. Only initiation reactions were disabled because it is sufficient to eliminate the reactions in which N_2 is broken due to their relatively high activation energies, except for the thermal pathway. For the thermal pathway, the entire pathway had to be disabled as subsequent reactions continued to take place and the overall error was higher when disabling only the initial reactions. As shown in section 4, the errors were low as emission values obtained by the sum of the calculated contributions is close to the total without any disabled reaction.

The disabled reactions for each mechanism can be found in Table 1. In the case of NO-reburning, reactions in which NO is consumed were disabled except those considered as initiation reactions (reversed) in any of the formation pathways.

The conceptual design of the ITB predicted an important role of reburning because the NO_x generated in the main combustor would be present in the oxidizer streams of the interturbine combustor. However, the oxidizer utilized during the experiments did not contain any NO_x and reburning took place due to recirculation within the combustor. The occurrence of reburning in FC conditions has been identified and discussed in the literature.[47]

3.4. Results. The results obtained with both CFD and CRN approaches in relation to overall emissions can be summarized by Figures 15−18. In these figures, prediction of emissions for the adiabatic and nonadiabatic CFD cases are shown along with the CRN results for both the GRI 3.0 and the GRI 2.11 chemical mechanisms.

The results for CO (Figures 15 and 17) show that the CFD simulations overpredict the emissions. The nonmonotonic behavior present in the experiments is not captured by the simulations. The over-prediction is either a result of limitations in the formulation of the employed FGM model or in the prediction of the mixing between the streams. The definition of the progress variable as a function of CO mass fraction could also be a source of error. However, the use of H_2O mass fraction to define the progress variable provided worse results. However, the CRN results are very close to the experimental

Table 1. Initiation Reactions of the Different NO_x Formation and Destruction Pathways

thermal		
$N + NO \rightleftarrows N_2 + O$	$N + O_2 \rightleftarrows NO + O$	$N + OH \rightleftarrows NO + H$
prompt		
$CH+N_2 \rightleftarrows HCN + N$	$C + N_2 \rightleftarrows CN + N$	$CH + N_2(+ M) \rightleftarrows HCNN (+ M)$
N_2O intermediate		
$N_2O + OH \rightleftarrows N_2 + HO_2$	$N_2O (+M) \rightleftarrows N_2 + O (+ M)$	
NNH		
$NNH \rightleftarrows N_2 + H$	$NNH (+M) \rightleftarrows N_2 + H (+M)$	$NNH + O_2 \rightleftarrows HO_2 + N_2$
NO reburning		
$C + NO \rightleftarrows CN + O$	$C + NO \rightleftarrows CO + N$	$CH + NO \rightleftarrows HCN + O$
$CH + NO \rightleftarrows H + NCO$	$CH + NO \rightleftarrows HCO + N$	$CH_2 + NO \rightleftarrows H + HNCO$
$H_2 + NO \rightleftarrows HCN + OH$	$CH_2 + NO \rightleftarrows H + HCNO$	$CH_2(S) + NO \rightleftarrows H + HNCO$
$CH_2(S) + NO \rightleftarrows HCN + OH$	$CH_3 + NO \rightleftarrows H_2O + HCN$	$CH_3 + NO \rightleftarrows H_2CN + OH$
$HCCO + NO \rightleftarrows CO + HCNO$	$HO_2 + NO \rightleftarrows NO_2 + OH$	$H + NO (+M) \rightleftarrows HNO (+M)$
$NO + O (+ M) \rightleftarrows NO_2 (+ M)$	$NO_2 + O \rightleftarrows NO + O_2$	

CO data, with little difference between the two chemical mechanisms, although the GRI 2.11 has marginally better predictions.

In the case of NO_x emissions (Figures 16 and 18), it is noteworthy to see how the adiabatic FGM highly over-predicts the values. Such behavior is expected, as heat losses were present in the experiments and NOx emissions depend on the peak temperatures. The nonadiabatic CFD approach has better predictions, being the best among the four approaches in capturing the effect of N_2 addition (Figure 18). However, it fails to predict the nonmonotonic behavior of NO_x emissions with increasing equivalence ratio (Figure 16).

The NO_x behavior is captured by the CRN for variations of Φ and N_2 addition. In accordance with previous works, the GRI 3.0 yields values as high as 10 times the experimental data points. Therefore, the best prediction for NO_x with a variation of equivalence ratio is obtained from the CRN with GRI 2.11, although still over-predicted. The unusual nonmonotonic behavior of NOx with increasing equivalence ratio can be explained by analyzing the NO_x-formation pathways, presented in section 4.

4. NO_X FORMATION ANALYSIS

The detailed chemistry incorporated in the CRN allows detailed analysis of the contributions from the different NO_x formation pathways. Figure 19 presents the relative and absolute contributions of the NOx formation pathways with a variation of Φ. Interestingly, the contribution of the thermal pathway is minor and invariant to some extent across all conditions.

When the emission values predicted with the GRI 2.11 mechanism and the sum of the calculated contributions in Figure 19 are compared, it can be noticed that the largest deviation occurs in cases in which the dominant pathways shift (around ϕ = 0.21 and ϕ = 0.24). The contributions of prompt NO formation and NO reburning are the key differences in relation to the NO_x emission at other equivalence ratios. Therefore, the interplay between prompt and reburning with

DOI: 10.1021/acs.energyfuels.7b02473
Energy Fuels 2018, 32, 822−838

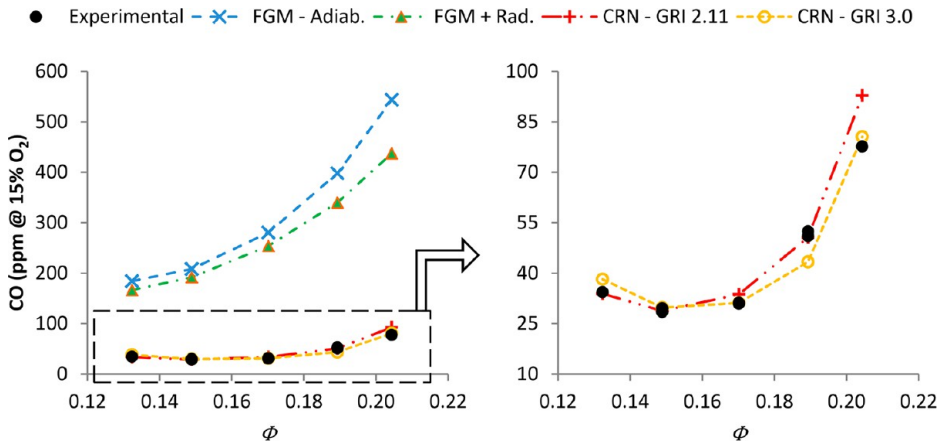

Figure 15. CO emissions as a function of the global equivalence ratio. Comparison between experimental data[30] and modeled results.

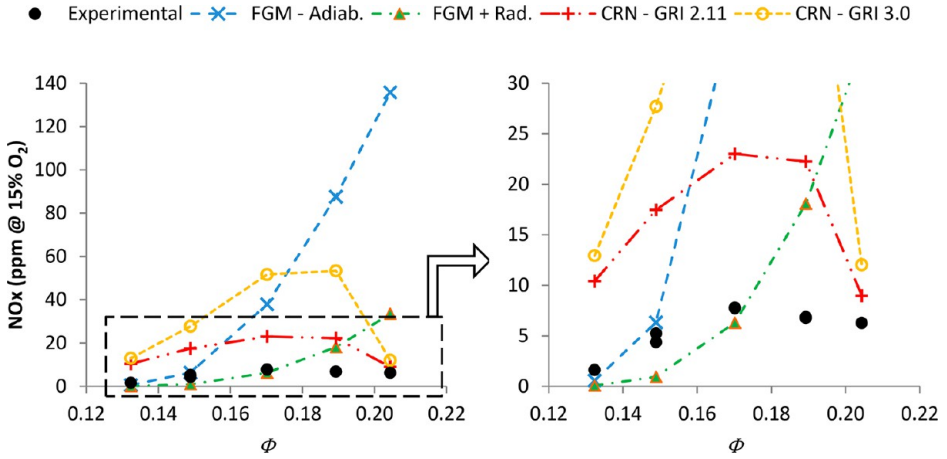

Figure 16. NO_x emissions as a function of the global equivalence. Comparison between experimental data[30] and modeled results.

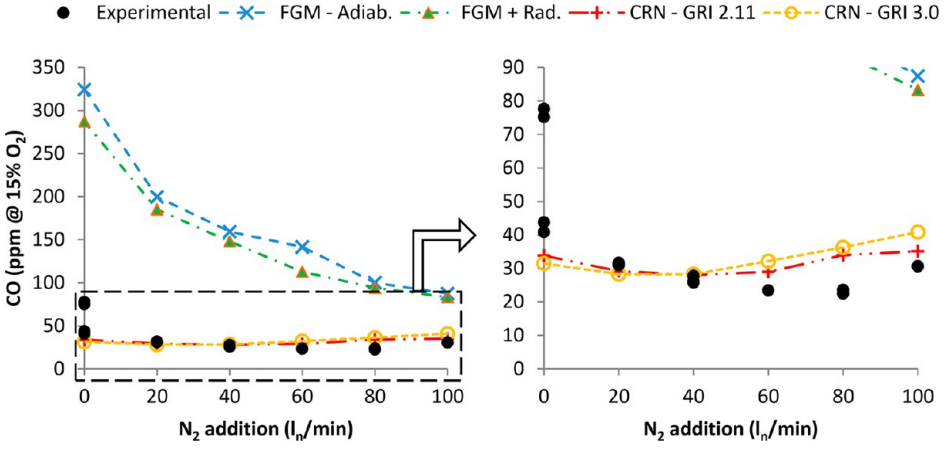

Figure 17. CO emissions as a function of N_2 addition to the oxidizer. Fixed fuel and air mass flow. Comparison between experimental data[30] and modeled results.

other pathways appear to be significant. One could argue that the calculation of NO reburning is probably responsible for the deviations, as more reactions have to be deactivated.

The overall behavior of the NO_x formation is dominated by prompt NOx. The initial NO_x increase with ϕ can be attributed to the prompt pathway, with a smaller contribution of the NNH pathway. Subsequently, NNH drops when the prompt reaches its peak (around ϕ = 0.24). A further increase in equivalence ratio reduces both NNH and prompt mechanism, as well as increases reburning, reducing the overall NO_x production.

The behavior of prompt NO_x in the CRN can be explained by analyzing the combustion PSRs (presented in Figures 13 and 14), where the most important reactions take place. A plot of the C-to-O mass ratio excluding CO_2 and H_2O (which indicate complete combustion) is shown in Figure 20 for the three PSRs. The C-to-O ratio in the Combustion 2 zone always increases with increasing ϕ. However, The C-to-O ratio in the

DOI: 10.1021/acs.energyfuels.7b02473
Energy Fuels 2018, 32, 822−838

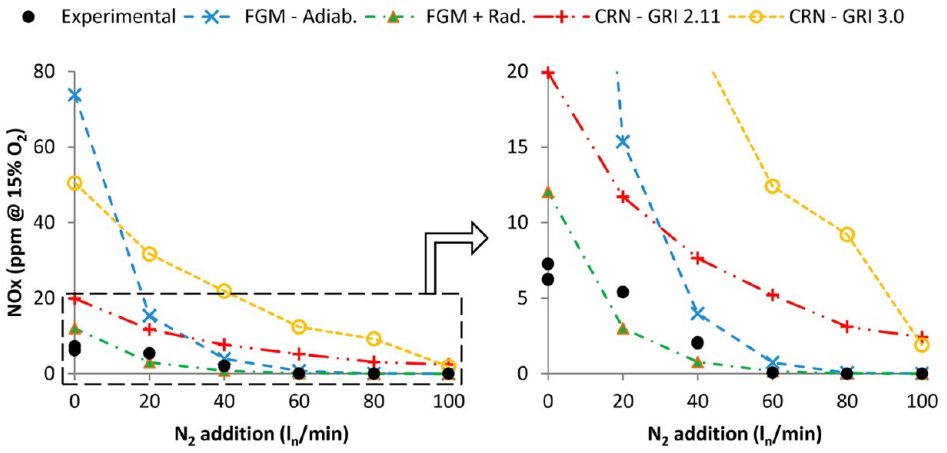

Figure 18. NO_x emissions as a function of N_2 addition to the oxidizer. Fixed fuel and air mass flow. Comparison between experimental data[30] and modeled results.

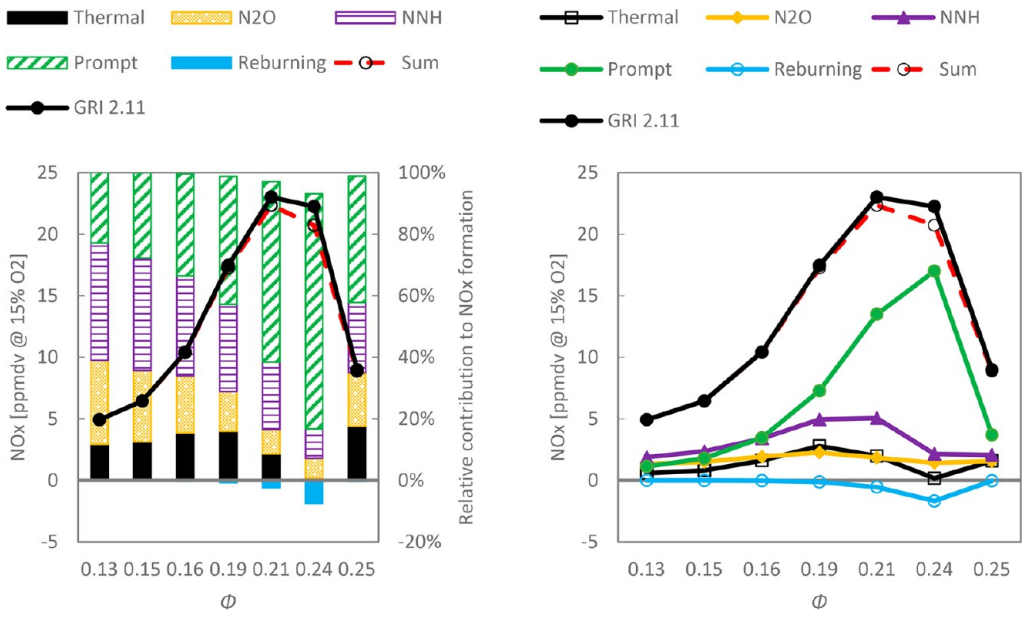

Figure 19. Relative (left) and absolute (right) contributions of NO_x formation pathways for different global equivalence ratios. Results from the CRN model with the GRI 2.11 mechanism.

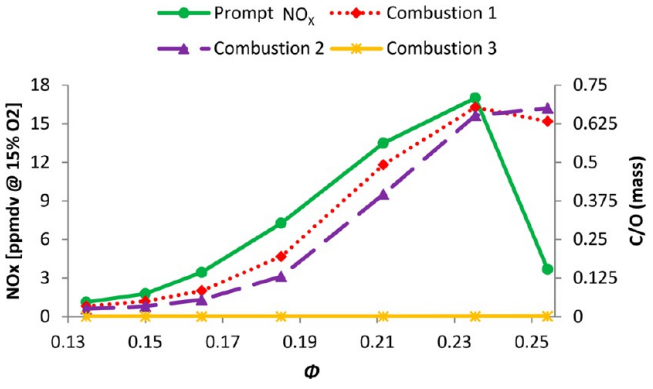

Figure 20. Prompt NO*x* emissions and the C-to-O mass ratio (excluding H_2O and CO_2) for the combustion PSRs as functions of the global equivalence ratio using the GRI 2.11 mechanism.

Combustion 1 reactor has similar behavior to that of prompt NO_x formation, decreasing for the highest ϕ. The C-to-O ratio may be regarded as a local equivalence ratio, neglecting the products of complete combustion. It aids the analysis because it is difficult to assess each reactor based on inlet values, as the CRN has several recirculations and interplays between the PSRs.

To further analyze prompt NO_x formation, the intermediate species HCN and CH are the most important.[48,49] The plots of their mass fractions in the Combustion 1 and 2 PSRs are presented in Figure 21. The results once again point to the importance of the reactions taking place in the Combustion 1 PSR, as both HCN and CH peak at the value of ϕ in which prompt emissions are the highest and drop dramatically with further increase in ϕ. Both species exhibit considerably lower concentrations in the Combustion 2 reactor and, while CH behaves similarly to the Combustion 1 reactor, HCN always increases with increasing ϕ. Therefore, it can be concluded that the overall NO_x behavior of the combustor is governed by the prompt pathway taking place in main reaction zone, close to the combustor wall.

DOI: 10.1021/acs.energyfuels.7b02473
Energy Fuels 2018, 32, 822−838

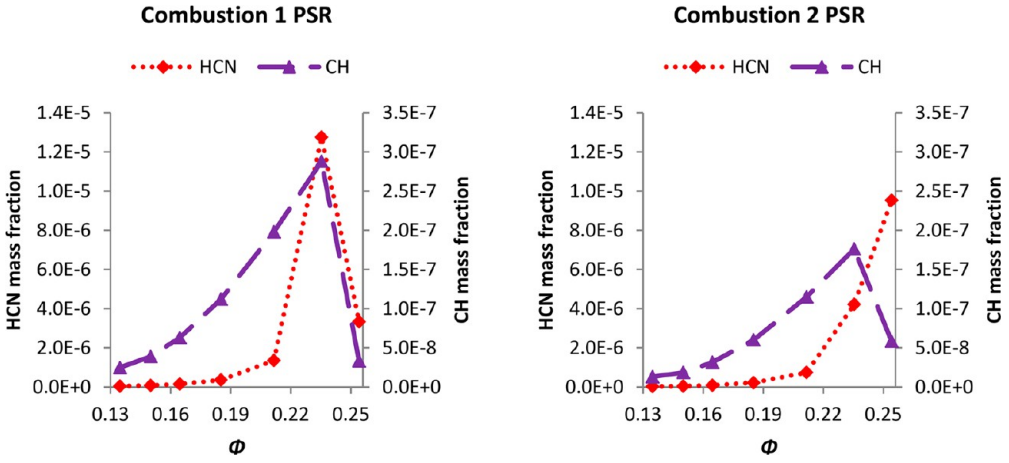

Figure 21. Mass fractions of HCN and CH in the combustion 1 (left) and combustion 2 (right) PSRs as a function of the global equivalence ratio using the GRI 2.11 mechanism.

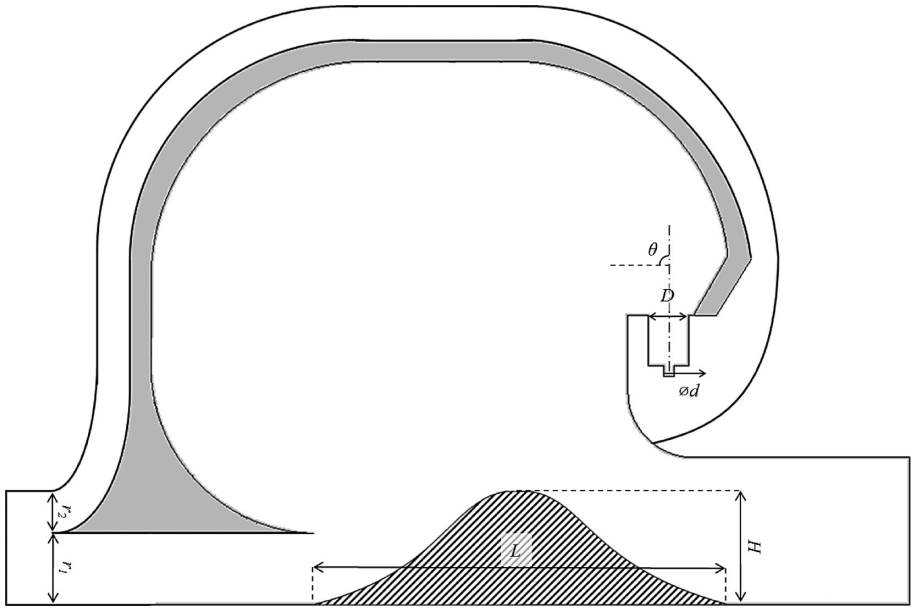

Figure 22. Dimensions that can be modified to improve the combustor design.

5. DESIGN MODIFICATIONS

The simulation results allow for the assessment of the designed combustor. A pair of undesirable features were observed through the simulations and, to some extent, with the experiments: (i) most reactions take place close to the combustor walls, and (ii) the dilution oxidizer does not enhance the recirculation within the combustor and does not mix properly with the products before leaving the combustor.

Figure 22 shows the dimensions that may be modified to improve the performance of the combustor. The direction of the fuel and combustion air streams (denoted by the angle θ), as well as the velocity of the jets, cause the reactions to occur close to the walls. The mixture impinges upon the combustor walls at high velocities. Reducing the velocity by increasing the diameter of the fuel (d) and oxidizer (D) ports could be an option but with a drawback of hindering the mixing between the streams due to the lower jet momentum. Altering the injection angle should also be considered, in particular making it point toward the intended recirculation zone.

Regarding the effect of the dilution oxidizer, more-complex modifications may be required. The designed split between combustion and dilution air was based on the assumption that dilution air would interact and enhance the recirculation, thereby homogenizing the flow leaving the combustor. The increase in the relative amount of dilution air would probably enhance mixing and could be performed by altering the ratio between r_1 and r_2. However, it would be unlikely that the problem would be solved without further modification of the geometry. An interesting option is to alter the direction of the dilution oxidizer flow by adding an obstacle between the dilution air inlet and the outlet of the combustor, as shown by the patterned area in Figure 22. The shape and dimensions (length and height) of this obstacle should be studied to enhance interaction with the recirculation zone while not excessively increasing pressure losses.

6. CONCLUSIONS

This work presented computational calculations related to an interturbine flameless combustor for gas turbines. The

DOI: 10.1021/acs.energyfuels.7b02473
Energy Fuels 2018, 32, 822−838

modeling was performed using both CFD and CRN approaches, and the results were compared to experimental data on the CO and NO_x emissions.

The conclusions of the analyses may be summarized as follows:

- The CRN model was better in predicting the pollutant emissions from the FC combustor than the CFD model.
- Both CFD simulations and experiments point to the occurrence of reactions close the combustor walls and not within the large recirculation zone, as envisioned by the conceptual design. Modifications in fuel injection position and direction, as well as air split, should be considered to improve the ITB design.
- The different levels of oxidizer dilution with N_2 lead the transition toward FC regime, as evidenced by the low Da in the simulations and spreading of the reaction zone observed during the experiments.
- The prompt NO_x formation mechanism is the dominant pathway and determines the overall of NO_x emissions behavior. The thermal pathway has a relatively low contribution, being less important than the NNH and N_2O-intermediate pathways.
- The joint application of CFD and CRNs is a better strategy by which to aid the combustor design, especially when pollutant emissions are important.
- The ITB design may be improved by assuring that the reactions take place in the main recirculation zone and that the dilution oxidizer stream is well-mixed before leaving the combustor.

AUTHOR INFORMATION

Corresponding Author

*E-mail: A.GangoliRao@tudelft.nl.

ORCID

Arvind Gangoli Rao: 0000-0002-9558-8171

Notes

The authors declare no competing financial interest.

ACKNOWLEDGMENTS

The authors would like to thank CNPq (National Counsel of Technological and Scientific Development - Brazil) support via the Science without Borders program and the European Union Seventh Framework Program (FP7/2007-2013) under grant agreement No. 284636 for the AHEAD project. The authors would also like to thank the partners involved in the Advanced Hybrid Engines for Aircraft Development, especially Prof. Mario Costa and Bruno Bernardes, IST Portugal, for facilitating the experiments.

ACRONYMS

AHEAD = Advanced Hybrid Engines for Aircraft Development
CFD = computational fluid dynamics
CRN = chemical reactor network
FC = flameless combustion
FGM = flamelet-generated manifolds
ITB = inter-turbine burner

LATIN SYMBOLS

A = area of the defined surface for calculating the recirculation ratio
c = progress variable
c_p = specific heat capacity at constant pressure (J/gK)
Da = Damköhler number
f = mixture fraction
H = enthalpy (J/kg)
k = turbulent kinetic energy (m^2/s^2)
Ka = Karlovitz number
l_t = turbulence length scale (m)
$\dot{m}$ = mass flow (kg/s)
$\mathbf{N}$ = unit vector normal to the area
p = β-shape probability density function
R = eecirculation ratio
S = source-term (kg/m^3s)
S_l = laminar flame speed (m/s)
T = temperature (K) integral scale
t = time (s)
u' = velocity fluctuation (m/s)
$\mathbf{V}$ = velocity vector
Y = mass fraction

GREEK SYMBOLS

α diffusivity (Lewis number = 1 (m^2/s)
ε turbulent dissipation rate (m^2/s^3)
ρ density (kg/m^3)
τ_c chemical time scale (s)
τ_t turbulence time scale (s)
ϕ global equivalence ratio
ϕ_{loc} local equivalence ratio (considering only the combustion oxidizer and not the dilution oxidizer)
χ scalar dissipation rate (1/s)

SUBSCRIPTS

L laminar flame
T temperature (K) integral scale
oxid oxidizer
loc local
i species

SUPERSCRIPTS

eq chemical equilibrium
u unburnt reactants

REFERENCES

(1) Airbus. *Navigating the Future: Global Market Forecast 2012-2031*; Airbus: Leiden, The Netherlands, 2012

(2) European Commission. *Flightpath 2050 Europe's Vision for Aviation*; Report of the high-level group on aviation research, Publications Office of the European Union; European Commission: Bruxelles, France, 2011

(3) Gohardani, A. S.; Doulgeris, G.; Singh, R. Challenges of future aircraft propulsion: A review of distributed propulsion technology and its potential application for the all electric commercial aircraft. *Prog. Aeronaut. Sci.* **2011**, *47*, 369−391.

(4) Cavaliere, A.; de Joannon, M. Mild Combustion. *Prog. Energy Combust. Sci.* **2004**, *30*, 329−366.

(5) Rao, A. G.; Levy, Y. A new combustion methodology for low emission gas turbine engines. *8th International Symposium on High-Temperature Air Combustion and Gasification*, Poznan, Poland, Jul 5−7, 2010.

(6) Lückerath, R.; Meier, W.; Aigner, M. FLOX combustion at high pressure with different fuel compositions. *J. Eng. Gas Turbines Power* **2008**, *130*, 11505.

(7) Lammel, O.; Schütz, H.; Schmitz, G.; Lückerath, R.; Stöhr, M.; Noll, B.; Aigner, M.; Hase, M.; Krebs, W. FLOX® combustion at high

DOI: 10.1021/acs.energyfuels.7b02473
Energy Fuels 2018, 32, 822−838

power density and high flame temperatures. *J. Eng. Gas Turbines Power* **2010**, *132*, 121503.
(8) Schütz, H.; Lammel, O.; Schmitz, G.; Rödiger, T.; Aigner, M. EZEE: a high power density modulating FLOX combustor. *Proceedings of ASME Turbo Expo*; ASME: Copenhagen, Denmark, 2012.
(9) Roediger, T.; Lammel, O.; Aigner, M.; Beck, C.; Krebs, W. Part-load operation of a piloted FLOX® combustion system. *J. Eng. Gas Turbines Power* **2013**, *135*, 31503.
(10) Zanger, J.; Monz, T.; Aigner, M. In *Experimental investigation of the combustion characteristics of a double-staged FLOX-based combustor on an atmospheric and a micro gas turbine test rig*; ASME Turbo Expo, Montreal, Canada, Jun 15−19, 2015.
(11) Zizin, A.; Lammel, O.; Severin, M.; Ax, H.; Aigner, M. In *Development of a jet-stabilized low-emission combustor for liquid fuels*; ASME Turbo Expo, Montreal, Canada, Jun 15−19, 2015.
(12) Gounder, J. D.; Zizin, A.; Lammel, O.; Aigner, M. In *Spray characteristics measured in a new FLOX based low emission combustor for liquid fuels using laser and optical diagnostics*; ASME Turbo Expo, Seoul, South Korea, Jun 13−17, 2016.
(13) Arghode, V. K.; Gupta, A. K. Role of thermal intensity on operational characteristics of ultra-low emission colorless distributed combustion. *Appl. Energy* **2013**, *111*, 930−956.
(14) Levy, Y.; Sherbaum, V.; Arfi, P. Basic thermodynamics of FLOXCOM, the low-NO_x gas turbines adiabatic combustor. *Appl. Therm. Eng.* **2004**, *24*, 1593−1605.
(15) Levy, Y.; Sherbaum, V.; Erenburg, V. In *Fundamentals of low-NOx gas turbine adiabatic combustor*; ASME Turbo Expo, Reno, NV, Jun 6−9, 2015.
(16) Levy, Y.; Sherbaum, V.; Erenburg, V. In *The role of the recirculating gases in the MILD combustion regime formation*; ASME Turbo Expo, Montreal, Canada, May 14−17, 2007.
(17) Melo, M. J.; Sousa, J. M. M.; Costa, M.; Levy, Y. Experimental investigation of a novel combustor model for gas turbines. *J. Propul. Power* **2009**, *25*, 609−617.
(18) Melo, M. J.; Sousa, J. M. M.; Costa, M.; Levy, Y. Flow and combustion characteristics of a low-NOx combustor model for gas turbines. *J. Propul. Power* **2011**, *27*, 1212−1217.
(19) Rao, A. G.; Yin, F.; van Buijtenen, J. P. A hybrid engine concept for multi-fuel blended wing body. *Aircr. Eng.* **2014**, *86*, 483−493.
(20) Rao, A. G.; Bhat, A. In *Hybrid combustion system for future aero engines*, 2nd National Propulsion Conference, Bombay, India, Feb 23−24, 2015.
(21) Yin, F.; Rao, A. G. Off-design performance of an interstage turbine burner turbofan engine. *J. Eng. Gas Turbines Power* **2017**, *139*, 82603.
(22) Levy, Y.; Erenburg, V.; Sherbaum, V.; Gaissinski, I. In *Flameless oxidation combustor development for a sequential combustion hybrid turbofan engine*; ASME Turbo Expo, Seoul, South Korea, Jun 13−17, 2016.
(23) Lyra, S.; Cant, R. S. Analysis of high pressure premixed flames using Equivalent Reactor Networks. *Fuel* **2013**, *107*, 261−268.
(24) Park, J.; Nguyen, T. H.; Joung, D.; Huh, K. Y.; Lee, M. C. Prediction of NOx and CO emissions from an industrial lean-premixed gas turbine combustor using a chemical reactor network model. *Energy Fuels* **2013**, *27*, 1643−1651.
(25) Lebedev, A. B.; Secundov, A. M.; Starik, A. M.; Titova, N. S.; Schepin, A. M. Modeling study of gas-turbine combustor emission. *Proc. Combust. Inst.* **2009**, *32*, 2941−2947.
(26) Monaghan, R. F. D.; Tahir, R.; Bourque, G.; Füri, M.; Gordon, R. L.; Faravelli, T.; Frassoldati, A.; Curran, H. J.; Cuoci, A. Detailed multi-dimensional study of pollutant formation in a methane diffusion flame. *Energy Fuels* **2012**, *26*, 1598−1611.
(27) Fichet, V.; Kanniche, M.; Plion, P.; Gicquel, O. A reactor network model for predicting NOx emissions in gas turbines. *Fuel* **2010**, *89*, 2202−2210.
(28) Cuoci, A.; Frassoldati, A.; Stagni, A.; Faravelli, T.; Ranzi, E.; Buzzi-Ferraris, G. Numerical modeling of NOx formation in turbulent flames using a kinetic post-processing technique. *Energy Fuels* **2013**, *27*, 1104−1122.
(29) Veríssimo, A. S.; Rocha, A. M. A.; Costa, M. Operational, combustion, and emission characteristics of a small-scale combustor. *Energy Fuels* **2011**, *25*, 2469−2480.
(30) Levy, Y.; Reichel, T. G. Feasibility of the hybrid combustion concept. *Advanced Hybrid Engines for Aircraft Development − Deliverable 2.7*; December, 2014.
(31) Tu, Y.; Su, K.; Liu, H.; Wang, Z.; Xie, Y.; Zheng, C.; Li, W. MILD combustion of natural gas using low preheating temperature air in an industrial furnace. *Fuel Process. Technol.* **2017**, *156*, 72−81.
(32) Dally, B. B.; Riesmeier, E.; Peters, N. Effect of fuel mixture on moderate and intense low oxygen dilution combustion. *Combust. Flame* **2004**, *137*, 418−431.
(33) van Oijen, J. A.; de Goey, P. H. Modelling of premixed laminar flames using flamelet-generated manifolds. *Combust. Sci. Technol.* **2000**, *161*, 113−137.
(34) Smith, G. P.; Golden, D. M.; Frenklach, M.; Moriarty, N. W.; Eiteneer, B.; Goldenberg, M.; Bowman, C. T.; Hanson, R. K.; Song, S.; Gardiner, Jr., W. C.; Lissianski, V. V.; Qin, Z. GRI-Mech Home Page. http://combustion.berkeley.edu/gri-mech/version30/text30.html (accessed April 2016).
(35) Modest, M. F. The weighted-sum-of-gray-gases model for arbitrary solution methods in radiative transfer. *J. Heat Transfer* **1991**, *113*, 650−656.
(36) Loenen, E.; van der Tempel, L. *Determination of absorption coefficients of glasses at high temperatures, by measuring the thermal emission*; Philips Research, Unclassified Report 020/96; Phillips Research: Eindhoven, The Netherlands, 1996.
(37) Galletti, C.; Parente, A.; Tognotti, L. Numerical and experimental investigation of a mild combustion burner. *Combust. Flame* **2007**, *151*, 649−664.
(38) Zimont, V.; Polifke, W.; Bettelini, M.; Weisenstein, W. In *An efficient computational model for premixed turbulent combustion at high Reynolds numbers based on a turbulent flame speed closure*; ASME International Gas Turbine and Aeroengine Congress and Exposition, Orlando, FL, Jun 2−5, 1997.
(39) Yin, F.; Rao, A. G. In *Performance analysis of an aero engine with interstage turbine burner*, 23rd International Society of Air-breathing Engines Conference, Manchester, United Kingdom, Sep 03−08, 2017.
(40) Goodwin, D. G.; Moffat, H. K.; Speth, R. L. Cantera: An object-oriented software toolkit for chemical kinetics, thermodynamics, and transport processes. http://www.cantera.org, Version 2.2.1, 2016 (accessed February 2016).
(41) Bowman, C. T.; Hanson, R. K.; Davidson, D. F.; Gardiner, Jr., W. C.; Lissianski, V.; Smith, G. P.; Golden, D. M.; Frenklach, M.; Goldenberg, M. http://combustion.berkeley.edu/gri-mech/new21/version21/text21.html (accessed September 2016).
(42) Lee, K. W.; Choi, D. H. Prediction of NO in turbulent diffusion flames using Eulerian particle flamelet model. *Combust. Theory Modell.* **2008**, *12*, 905−927.
(43) Barlow, R. S.; Karpetis, A. N.; Frank, J. H.; Chen, J.-Y. Scalar profiles and NO formation in laminar opposed-flow partially premixed methane/air flames. *Combust. Flame* **2001**, *127*, 2102−2118.
(44) Kim, S. H.; Huh, K. Y.; Dally, B. Conditional moment closure modeling of turbulent nonpremixed combustion in diluted hot coflow. *Proc. Combust. Inst.* **2005**, *30*, 751−757.
(45) Nicol, D. G.; Steele, R. C.; Marinov, N. M.; Malte, P. C. In *The importance of the nitrous oxide pathway to NO_x in lean-premixed combustion*; ASME International Gas Turbine and Aeroengine Congress and Exposition, Cincinnati, OH, May 24−27, 1993.
(46) Guethe, F.; García, M. C.; Burder, A. In *Flue gas recirculation in gas turbine: investigation of combustion reactivity and NO_x emission*; ASME Turbo Expo, Orlando, FL, Jun 8−12, 2009.
(47) Nicolle, A.; Dagaut, P. Occurrence of NO-reburning in MILD combustion evidenced via chemical kinetic modeling. *Fuel* **2006**, *85*, 2469−2478.
(48) Hewson, J. C.; Bollig, M. Reduced mechanisms for NOx emissions from hydrocarbon diffusion flames. *Symp. (Int.) Combust., [Proc.]* **1996**, *26*, 2171−2179.

DOI: 10.1021/acs.energyfuels.7b02473
Energy Fuels 2018, 32, 822−838

(49) Zhao, D.; Yamashita, H.; Kitagawa, K.; Arai, N.; Furuhata, T. Behavior and effect on NOx formation of OH radical in methane-air diffusion flame with steam addition. *Combust. Flame* **2002**, *130*, 352−360.

DOI: 10.1021/acs.energyfuels.7b02473
Energy Fuels 2018, 32, 822−838